1000-0569/2013/029(10)-3323-35 *Acta Petrologica Sinica* 岩石学报

巴楚辉绿岩墙的岩石成因及其对塔里木大火成岩省岩浆演化的启示*

位荀[1,2] 徐义刚[1**]

WEI Xun[1,2] and XU YiGang[1**]

1. 中国科学院广州地球化学研究所 同位素地球化学国家重点实验室, 广州 510640

2. 中国科学院大学,北京 100039

1. *State Key Laboratory of Isotope Geochemistry*, *Guangzhou Institute of Geochemistry*, *Chinese Academy of Sciences*, *Guangzhou* 510640, *China*

2. *University of Chinese Academy of Sciences*, *Beijing* 100039, *China*

2013-04-20 收稿, 2013-07-03 改回.

Wei X and Xu YG. 2013. Petrogenesis of the mafic dykes from Bachu and implications for the magma evolution of the Tarim large igneous province, NW China. *Acta Petrologica Sinica*, 29(10):3323 – 3335

Abstract The Early Permian Tarim large igneous province (TLIP) in Northwest China consists of two main magmatic phases: the earlier one (~290Ma) represented by basalts in Keping, and the later one (~280Ma) by ultramafic-mafic-felsic intrusions and mafic dykes in Bachu. In order to identify mantle and crustal components involved in the genesis of the TLIP and to understand the plume-lithosphere interaction, we performed zircon U-Pb dating, geochemical analyses on the Bachu dykes. Zircons from sample XHZ-10 are all inherited in origin, thus yielding no constraints on eruption age. Field relationship, however, suggests that the Bachu dykes were emplaced during the second episode of TLIP magmatism. The Bachu dykes experienced fractionation of olivine, clinopyroxene and magnetite. Correlations among ε_{Nd} and SiO_2 and La/Nb, as well as the age spectrum of inherited zircons (2480 ~ 717Ma, with a peak at ~800Ma) suggest that some dykes with low ε_{Nd} may have been assimilated by Neoproterozoic basements en route to the surface. Nevertheless, the least-contaminated samples show OIB-like trace element compositions and high ε_{Nd} (~ +5), consistent with a derivation from a convective mantle source. This is in contrast with the earlier phase of magmatism (~290Ma), which was mainly derived from an enriched sub-continental lithospheric mantle (SCLM). We propose here a model involving plume lateral deflection to account for these two discrete magmatic phases in the TLIP. The earlier phase formed as a response of impact of a mantle plume at the base of the SCLM. Partial melting of the enriched lithospheric mantle was triggered by conductive heating of the impregnating plume. The later phase was generated by decompression melting of the mantle plume, as a result of deflection of the plume towards the margins of the Tarim craton where the lithosphere is relatively thin.

Key words Tarim; Large igneous province; Bachu dykes; Plume lateral deflection

摘 要 早二叠世塔里木大火成岩省主要有两期岩浆活动:以柯坪玄武岩为代表的喷出岩形成较早(~290Ma),以巴楚超基性-基性-长英质侵入体和岩墙为代表的侵入岩形成较晚(~280Ma)。本研究选取代表晚期岩浆活动的巴楚辉绿岩墙为研究对象,旨在为认识塔里木地幔柱活动及与岩石圈的相互作用提供更多信息。巴楚辉绿岩 XHZ-10 样品中的锆石均为继承性锆石,不能用来限定其侵位时代。然而,野外关系表明巴楚辉绿岩墙属于塔里木大火成岩省的第二期岩浆活动。巴楚辉绿岩墙经历了橄榄石、辉石和磁铁矿的分离结晶。Nd 同位素比值与 SiO_2 和 La/Nb 比值的相关性以及继承性锆石年龄(2480 ~ 717Ma,主要集中在~800Ma)表明,新元古代基底的同化混染作用可以解释其 ε_{Nd} 具有较大的变化范围(-2.6 ~ +5.1)。受混染程度最小的样品具有与洋岛玄武岩(OIB)极其相似的微量元素特征,并且具有亏损的 Nd 同位素组成(ε_{Nd} = ~ +5),暗示其来源于富集的对流地幔源区,与早期(~290Ma)具有岩石圈地幔源区特征的玄武岩形成鲜明对比。本文提出地幔柱侧向流动模型以解释两期岩浆的时空分布和地球化学差异:当地幔柱上升至塔里木岩石圈底部时,巨厚的岩石圈地幔(>140km)会阻碍其减压熔融;但不断积累在岩石圈底部的地幔柱物质提供足够的热,促使早期富集交代的岩石圈地幔发生部分熔融,形

* 本文受国家 973 项目(2011CB808906)资助.

第一作者简介: 位荀,男,1984 年生,博士生,岩石地球化学专业, E-mail: weixun@ yeah. net

** **通讯作者**:徐义刚,男,1966 年生,研究员,博士生导师,岩石地球化学专业, E-mail:yigangxu@ gig. ac. cn

成~290Ma 的玄武岩;地幔柱物质将向岩石圈厚度较薄的边缘地区侧向流动,发生减压熔融,形成的熔体侵位到地壳中形成超基性-基性-长英质侵入岩和辉绿岩墙,并诱发地壳的熔融形成长英质火山岩。

关键词 塔里木;大火成岩省;巴楚岩墙;地幔柱侧向流动

中图法分类号 P588.124

1 引言

大火成岩省主要由分布广泛(>10^5km^2)和巨量(>10^5km^3)的基性岩浆岩,以及少量相伴生的碱性长英质和硅不饱和岩浆岩组成,其持续时间最长可达50Myr,主体在较短(1~5Myr)的时间内形成(Bryan and Ernst, 2008)。其形成通常和地幔柱活动相关(Campbell, 2005; Campbell and Griffiths, 1990; Courtillot *et al.*, 2003; Griffiths and Campbell, 1990; Hill *et al.*, 1992; Richards *et al.*, 1989; Wolfe *et al.*, 2009; Xu *et al.*, 2004)。

早二叠世塔里木大火成岩省岩浆岩覆盖面积超过250000km^2(Tian *et al.*, 2010; Yang *et al.*, 2007),主要由分布在在盆地内部的溢流玄武岩和分布在盆地边缘的超基性-基性-长英质侵入体、长英质火山岩和基性岩墙组成(陈汉林等, 1997; 姜常义等, 2004; 厉子龙等, 2008; 杨树峰等, 2006; Tian *et al.*, 2010; Yang *et al.*, 2007; Yu *et al.*, 2011b; Zhang *et al.*, 2008, 2010a, b; 张洪安等, 2009)。在空间分布上不同的这两类岩浆在时间上也存在明显的差异:以柯坪玄武岩为代表的喷出岩形成较早(~290Ma),以巴楚超基性-基性-长英质侵入岩和岩墙为代表的侵入岩形成较晚(~280Ma)(位荀和徐义刚, 2011; 徐义刚等, 2013; Li *et al.*, 2011)。而且两期岩浆具有明显不同的地球化学特征:玄武岩具有 Nb-Ta 负异常和富集的 Nd 同位素组成,而侵入岩和岩墙具有 Nb-Ta 正异常和相对亏损的 Nd 同位素组成(Zhang *et al.*, 2010a; Zhou *et al.*, 2009)。尽管很多学者提出地幔柱模式来解释塔里木大火成岩省的形成(厉子龙等, 2008; Zhang *et al.*, 2010a; Zhou *et al.*, 2009),但现有模型并未很好地解释两期岩浆的时间、空间分布特征以及它们之间地球化学差异。

岩石圈-地幔柱的相互作用,在大火成岩省的形成过程中扮演了非常重要的角色(Gibson *et al.*, 1995, 1999, 2006; Molzahn *et al.*, 1996; Pik *et al.*, 1999)。柯坪玄武岩可能来自于富集的岩石圈地幔(Zhang *et al.*, 2010a),而巴楚辉绿岩墙源自富集的软流圈地幔(Zhou *et al.*, 2009);随着时间的演化,软流圈组分在塔里木岩浆岩中越来越明显,因此两期岩浆的形成可能与岩石圈-地幔柱的相互作用密切相关。巴楚岩墙具有较大的 ε_{Nd} 变化范围(-2.6~+5.1),可能是地壳同化混染也可能是岩石圈地幔物质不断加入所致,对这种现象的解释对理解塔里木大火成岩省形成过程中地幔柱和岩石圈的相对贡献以及相互作用具有重要的意义。

因此,本文对巴楚岩墙进行了锆石年代学和主量、微量元素分析,讨论其岩石成因及岩石圈和地幔柱在塔里木大火成岩省形成过程中的相对贡献;结合文献资料,提出地幔柱侧向流动模型解释两期岩浆的时间、空间分布特征,以及它们之间的地球化学差异。

2 区域地质背景和样品特征

塔里木盆地位于中国的西北部,覆盖面积超过600000km^2,被北部的天山造山带、南部的昆仑山和阿尔金造山带所围绕(图1b)。塔里木地块主要由前寒武纪的基底和上覆的古生代沉积地层组成(新疆维吾尔自治区地质矿产局, 1993)。前寒武纪基底主要形成于太古代、古元古代、中元古代和新元古代,主要出露在盆地边缘的库鲁克塔格、阿克苏-乌什、铁克里克等地区(新疆维吾尔自治区地质矿产局, 1993; 张师本, 2003)。塔里木盆地的岩浆期次主要有太古代、元古代和早二叠世(新疆维吾尔自治区地质矿产局, 1993; Hu *et al.*, 2000; Long *et al.*, 2010)。其中早二叠世的岩浆活动最为广泛,形成了大规模的溢流玄武岩、超基性-基性侵入岩、基性岩墙群和 A-型花岗岩类等(新疆维吾尔自治区地质矿产局, 1993; 杨树峰等, 2006; 厉子龙等, 2008; Zhang *et al.*, 2008, 2010a),覆盖面积约 2.5×10^5~3.0×10^5km^2(Tian *et al.*, 2010; Yang *et al.*, 2007)。玄武岩主要分布于盆地内部,分为底部的库普库兹曼组和上覆的开派兹雷克组,主要出露于柯坪和塔西南地区;超基性-基性侵入岩、基性岩墙群和 A-型花岗岩类主要出露于盆地边缘的巴楚、皮羌等地区。

研究区麻扎尔塔格地区(也称为小海子地区),位于塔里木盆地西北缘(图1a)。该区地层大部分被第四系覆盖,在小海子水库附近有零星出露,主要有志留系、泥盆系、石炭系以及早二叠统(新疆维吾尔自治区地质矿产局, 1993; 张师本, 2003)。该区出露早二叠世超基性-基性-长英质侵入岩组合、辉绿岩墙和石英正长斑岩脉。研究程度较高的小海子正长岩体,侵入到石炭系-早二叠统,呈近等轴圆形。年代学研究表明,正长岩形成于~280Ma(杨树峰等, 1996, 2006; 位荀和徐义刚, 2011)。正长岩体的边部有少数橄榄辉长岩堆晶岩。辉绿岩墙和石英正长斑岩脉不仅侵入到围岩地层中,也侵入到小海子正长岩体中,并且辉绿岩墙和正长岩局部有岩浆混合的现象(陈咪咪等, 2010; 张自力等, 2008),暗示辉绿岩墙可能和正长岩近同时侵位。

所采辉绿岩墙样品具有辉绿结构。斑晶主要为斜长石(<5%),基质主要由单斜辉石、斜长石和磁铁矿组成。样品均发生不同程度的蚀变:斜长石蚀变成绢云母,单斜辉石蚀

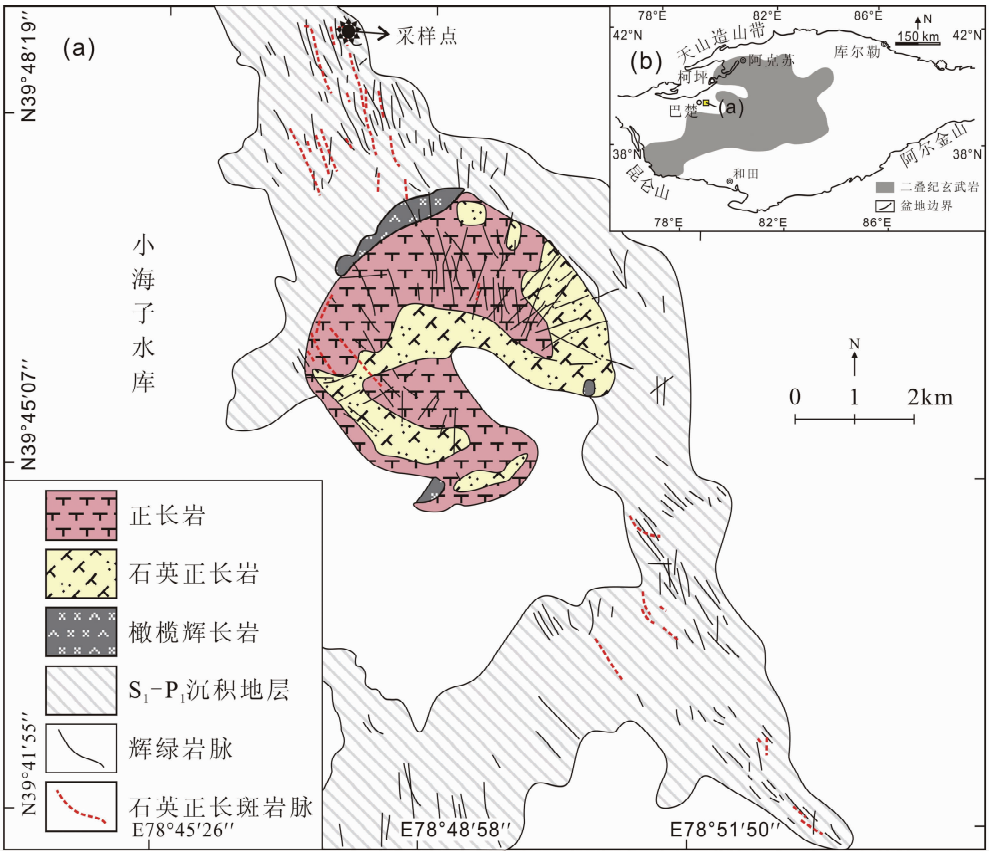


图 1 塔里木盆地(b)和巴楚小海子地区(a)地质简图(据 Yang *et al.*, 2007;陈咪咪等,2010 修改)

Fig. 1 Simplified geological map of the Tarim basin (b) and Bachu Xiaohaizi area (a) (modified after Yang *et al.*, 2007; Chen *et al.*, 2010)

变成不透明矿物。

3 分析方法

用于 U-Pb 年龄测定的样品 XHZ-10 用常规的重选和磁选技术分选出锆石。将锆石样品颗粒和锆石标样 Plésovice (Sláma *et al.*, 2008) 和 Qinghu (Li *et al.*, 2009) 粘贴在环氧树脂靶上,然后抛光使其曝露一半晶面。对锆石进行透射光和反射光显微照相以及阴极发光图象分析,以检查锆石的内部结构、帮助选择适宜的测试点位。阴极发光图像在中国科学院地质与地球物理研究所 LEO 1450 VP 扫描电镜上完成,分析电压为 15kV,电流为 1.1nA。

U、Th、Pb 的测定在中国科学院地质与地球物理研究所 CAMECA IMS-1280 二次离子质谱仪上进行,详细分析方法见 Li *et al.* (2009)。锆石标样与锆石样品以 1∶3 比例交替测定。U-Th-Pb 同位素比值用标准锆石 Plésovice (Sláma *et al.*, 2008) 校正获得,U 含量采用标准锆石 91500 (Wiedenbeck *et al.*, 1995) 校正获得,以长期监测标准样品获得的标准偏差(1SD = 1.5%, Li *et al.*, 2010)和单点测试内部精度共同传递得到样品单点误差,以标准样品 Qinghu (Li *et al.*, 2009) 作为未知样监测数据的精确度。普通 Pb 校正采用实测 ^{204}Pb 值。由于测得的普通 Pb 含量非常低,假定普通 Pb 主要来源于制样过程中带入的表面 Pb 污染,以现代地壳的平均 Pb 同位素组成(Stacey and Kramers, 1975) 作为普通 Pb 组成进行校正。同位素比值及年龄误差均为 1σ。数据结果处理采用 ISOPLOT 软件(Ludwig, 2003)。

主量和微量元素分析均在中国科学院广州地球化学研究所同位素地球化学国家重点实验室完成。主量元素在 Rigaku ZSX100e 仪器上完成,详细的分析方法见 Li *et al.* (2006)。大多数主量元素的分析精度在 1% ~5%。微量元素测定在 PE Elan 6000 型电感耦合等离子体质谱仪(ICP-MS)上完成,分析方法见 Xu (2002)。微量元素分析精度通常优于 5%。

4 分析结果

4.1 锆石 SIMS U-Pb 年代学

样品(XHZ-10)中的锆石,大部分为碎片;少数晶型完整的锆石呈长柱状,粒径 < 100μm。阴极发光(CL)图像(图 2a 中插图) 上具有典型的岩浆震荡环带和扇形环带, 暗示它们

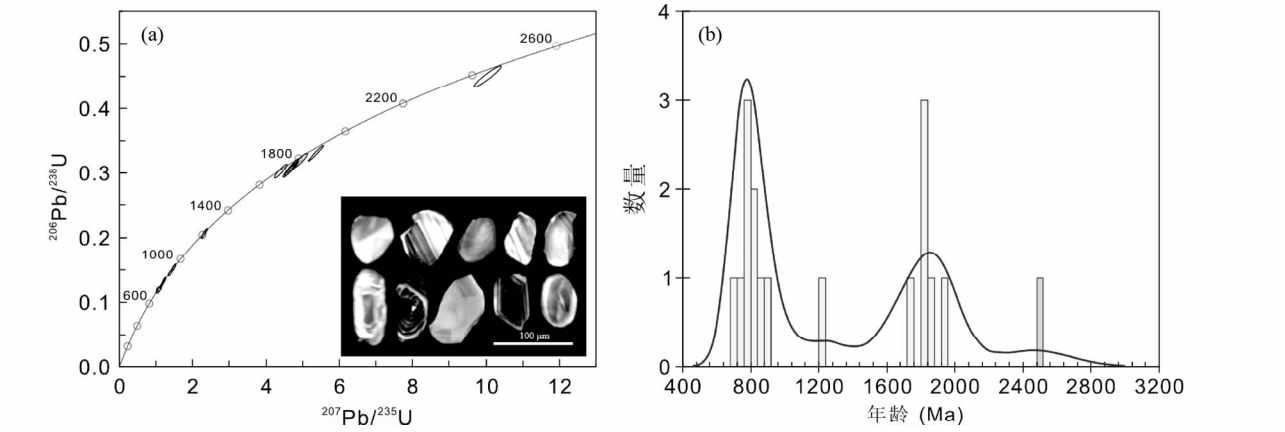


图 2 XHZ-10 样品锆石 U-Pb 协和图(a)和年龄分布直方图(b)

Fig. 2 U-Pb concordia diagram (a) and histogram (b) for zircons from XHZ-10

表 1 巴楚岩墙 XHZ-10 SIMS 锆石 U-Pb 年龄分析结果

Table 1 SIMS zircon U-Pb results of the Bachu dyke XHZ-10

测点号	U ($\times10^{-6}$)	Th ($\times10^{-6}$)	Th/U	f_{206} (%)	比值						年龄(Ma)					
					$^{207}Pb/^{206}Pb$	±1σ (%)	$^{207}Pb/^{235}U$	±1σ (%)	$^{206}Pb/^{238}U$	±1σ (%)	$^{207}Pb/^{206}Pb$	±1σ (%)	$^{207}Pb/^{235}U$	±1σ (%)	$^{206}Pb/^{238}U$	±1σ (%)
XHZ-10@01	245	120	0.49	0.01	0.1105	0.45	4.723	1.57	0.3100	1.50	1808	8	1771	13	1741	23
XHZ-10@02	287	183	0.64	0.10	0.0666	0.90	1.221	1.75	0.1329	1.50	826	19	810	10	805	11
XHZ-10@03	286	446	1.56	0.04	0.0660	0.90	1.171	1.75	0.1286	1.50	807	19	787	10	780	11
XHZ-10@04	329	181	0.55	0.03	0.0702	0.94	1.483	1.77	0.1533	1.50	933	19	923	11	919	13
XHZ-10@05	506	110	0.22	0.01	0.1178	0.31	5.357	1.56	0.3298	1.52	1923	6	1878	13	1838	24
XHZ-10@06	151	173	1.14	0.04	0.0662	1.26	1.075	1.96	0.1177	1.50	814	26	741	10	717	10
XHZ-10@07	159	89	0.56	0.10	0.1109	0.60	4.646	1.62	0.3038	1.50	1815	11	1758	14	1710	23
XHZ-10@8	88	76	0.86	0.01	0.0651	2.02	1.082	2.55	0.1206	1.56	777	42	745	14	734	11
XHZ-10@9	267	163	0.61	0.04	0.1116	0.46	4.695	1.57	0.3051	1.50	1826	8	1766	13	1717	23
XHZ-10@10	397	192	0.48	0.02	0.0692	0.99	1.387	1.80	0.1454	1.50	904	20	884	11	875	12
XHZ-10@11	275	204	0.74	0.03	0.0659	0.88	1.211	1.74	0.1332	1.50	803	18	805	10	806	11
XHZ-10@12	515	239	0.47	0.03	0.0662	0.68	1.169	1.65	0.1281	1.50	812	14	786	9	777	11
XHZ-10@13	346	47	0.13	0.05	0.0814	0.57	2.319	1.61	0.2067	1.50	1231	11	1218	11	1211	17
XHZ-10@14	1024	254	0.25	0.01	0.0659	0.44	1.187	1.56	0.1307	1.50	802	9	795	9	792	11
XHZ-10@15	234	82	0.35	0.02	0.1126	0.65	4.933	1.64	0.3179	1.50	1841	12	1808	14	1779	23
XHZ-10@16	234	94	0.40	0.22	0.1059	0.57	4.406	1.61	0.3018	1.50	1730	10	1713	13	1700	22
XHZ-10@17	116	93	0.80	0.06	0.1624	0.49	10.045	1.58	0.4487	1.50	2480	8	2439	15	2390	30

注:f_{206}为普通^{206}Pb占总^{206}Pb的比例

为岩浆成因锆石。这些锆石的 U、Th 变化范围分别为 $88\times10^{-6}\sim1024\times10^{-6}$,$47\times10^{-6}\sim446\times10^{-6}$,Th/U 比值为 0.13~1.56(表 1),符合岩浆锆石的特征。17 个分析点给出的协和年龄具有较大的变化范围(2480~717Ma;表 1、图 2)。

4.2 主量和微量元素

巴楚岩墙的 SiO_2 含量范围为 47%~51%,全碱(Na_2O+K_2O)变化范围较大(3.8%~7.0%)(除样品 XHZ-10 外)(表 2)。在抗蚀变元素判别图解($Zr/TiO_2\times0.0001$-Nb/Y)(图 3;Winchester and Floyd, 1977)上,这些样品位于碱性玄武岩区域。

这些样品(除样品 XHZ-10 外)具有较高的 TiO_2 含量(3.1%~3.8%)和 Ti/Y 比值(553~756),和峨眉山大火成岩省的高钛玄武岩相似(Xu *et al.*, 2001)。MgO 含量相对较低(3.5%~4.8%),$Mg^{\#}[(100Mg/(Mg+Fe^{2+})]$为 38~39,暗示它们经历了较为明显的分离结晶。在 Harker 图解(图 4)上,TiO_2、$Fe_2O_3{}^{T}$ 和 CaO 与 MgO 呈正相关,而 Al_2O_3 与 MgO 呈负相关。这些样品具有较低的 Sc($14.3\times10^{-6}\sim21.5\times10^{-6}$)、Cr($4.72\times10^{-6}\sim54.6\times10^{-6}$)和 Ni($20.5\times10^{-6}\sim56.5\times10^{-6}$)含量。

在稀土元素球粒陨石标准化图解(图 5a)上,巴楚岩墙

表 2 巴楚岩墙主量元素(wt%)XRF 和微量元素($\times 10^{-6}$) ICP-MS 分析结果

Table 2 Major (wt%) and trace elements ($\times 10^{-6}$) analysis results of the Bachu dykes

样品号	XHZ-8	XHZ-10	XHZ-13	XHZ-14
SiO_2	46.55	60.35	45.68	50.30
TiO_2	3.56	1.45	3.80	3.13
Al_2O_3	14.47	15.27	13.45	16.08
$Fe_2O_3^T$	14.17	7.68	14.74	12.08
MnO	0.24	0.15	0.16	0.16
MgO	4.42	3.40	4.76	3.50
CaO	6.64	2.09	8.67	8.97
Na_2O	3.50	2.54	2.18	3.34
K_2O	3.33	3.56	1.41	1.40
P_2O_5	1.02	0.21	0.52	0.46
L.O.I	1.61	3.02	4.20	0.19
Total	99.51	99.74	99.58	99.62
Sc	14.3	16.0	21.5	20.8
V	211	152	325	228
Cr	4.72	95.6	9.92	54.6
Co	44.1	34.1	53.4	31.0
Ni	33.2	60.8	56.5	20.5
Cu	56.8	59.4	99.0	24.5
Zn	187	245	161	147
Ga	31.1	21.8	25.1	26.0
Rb	122	74.6	22.9	34.8
Sr	840	366	615	673
Y	39.5	27.8	31.7	32.6
Zr	396	232	270	279
Nb	66.0	18.4	44.1	42.9
Cs	3.94	0.32	0.57	0.61
Ba	940	1424	752	581
La	114	43.4	39.2	40.5
Ce	220	88.9	84.7	88.1
Pr	26.1	10.3	10.7	10.9
Nd	99.1	38.7	44.0	45.9
Sm	17.1	7.02	9.15	9.48
Eu	4.87	1.73	2.87	3.05
Gd	14.4	6.30	8.65	8.68
Tb	1.87	0.93	1.26	1.28
Dy	8.60	4.96	6.46	6.66
Ho	1.38	0.95	1.17	1.15
Er	3.15	2.59	2.79	2.83
Tm	0.36	0.36	0.36	0.37
Yb	2.09	2.38	2.20	2.28
Lu	0.27	0.36	0.31	0.33
Hf	9.90	6.26	7.27	7.13
Ta	3.87	1.31	3.01	2.81
Th	8.44	9.85	4.69	4.67
U	2.20	1.73	1.13	1.14

具有右倾的 REE 分布模式：富集轻稀土(LREE)、亏损重稀土(HREE)，其$(La/Yb)_N$比值为 17.8 ~ 18.2。除 XHZ-10 外，没有明显的 Eu 异常。在原始地幔标准化图解(图 5b)中，大离子亲石元素(LILE；如 Rb、Ba、Th、U)和高场强元素(HFSE；如 Zr、Hf、Ti)富集，具有 Nb 和 Ta 的正异常，和洋岛玄武岩(OIB)具有非常相似的地球化学特征(Sun and McDonough，1989)。与其它几个样品不同，XHZ-10 具有明显的 Eu 负异常和 Nb-Ta 负异常。

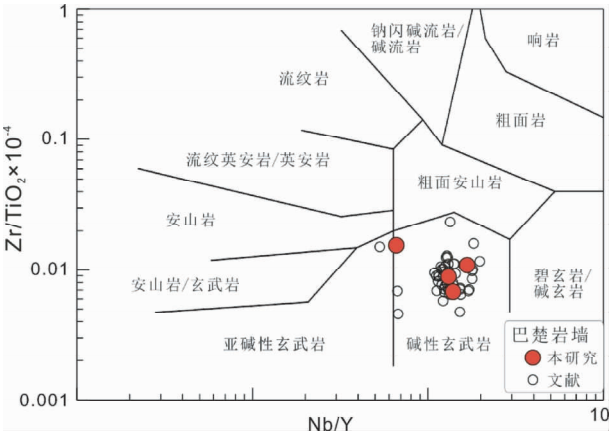


图 3 巴楚岩墙的 Nb/Y-$Zr/TiO_2\times10^{-4}$图解(文献数据据 Yang *et al.*，2007；Zhang *et al.*，2010a；Zhou *et al.*，2009)

Fig. 3 Plot of Nb/Y vs. $Zr/TiO_2\times10^{-4}$ for the Bachu dykes (Reference data after Yang *et al.*, 2007; Zhang *et al.*, 2010a; Zhou *et al.*, 2009)

5 讨论

5.1 锆石 SIMS U-Pb 年龄意义

锆石 SIMS U-Pb 年龄给出比较老的年龄(2480 ~ 717Ma)，在年龄分布直方图上显示有两个明显的峰，分别为 800Ma 和 1850Ma(图 2b)。巴楚岩墙侵入到石炭系-早二叠统，这些锆石年龄明显早于地层的形成时代，因此不能代表岩墙的结晶年龄。可能是岩墙在侵位过程中，捕虏周围围岩中的锆石，反映基底的信息。

5.2 蚀变影响

巴楚岩墙中一些样品具有相对高的 LOI(1.61% ~ 4.20%)，并且 Rb 和 Ba 等活动性元素和在蚀变过程中被认为最为稳定的元素 Zr 没有明显的相关性(图 6a 和 b)，暗示这些元素受到了蚀变的影响。而 Nb(图 6c)、U(图 6d)和 REE(未显示)等元素具有很好的正相关关系，暗示这些元素并未明显受到蚀变的影响，那么这些元素可以用来探讨它们的源区特征。

5.3 分离结晶

巴楚岩墙具有比较低的 MgO 含量和 $Mg^{\#}$，表明它们经历了比较明显的镁铁质矿物(如橄榄石、辉石)的分离结晶。在 Harker 图解(图 4)上，巴楚岩墙的 TiO_2 和 $Fe_2O_3^T$ 与 MgO 呈正相关，暗示有 Ti-Fe 氧化物的分离结晶；随着 MgO 的降低，

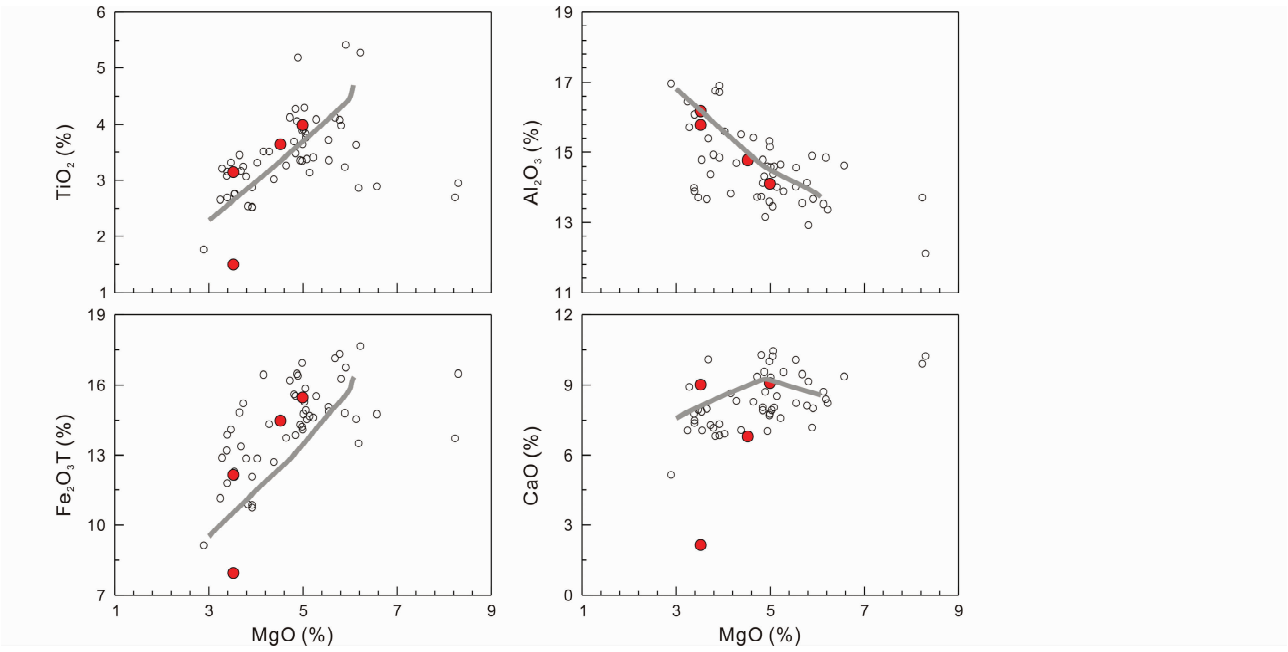


图 4 巴楚岩墙的 Harker 图解

灰色实线为 MELTS 模拟分离结晶趋势线. 图例和文献数据同图 3

Fig. 4 Harker diagrams of the Bachu dykes

The grey lines represent the results of the MELTS calculations of fractional crystallization. Symbols and reference data sources same as Fig. 3

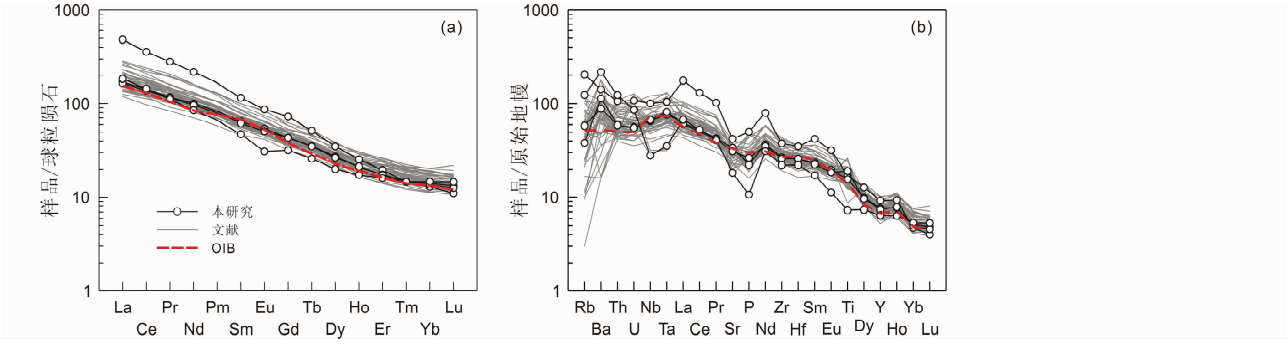


图 5 巴楚岩墙的稀土元素球粒陨石标准化图解(a)和微量元素原始地幔标准化蛛网图(b)(标准化值据 McDonough and Sun, 1995)

文献数据同图 3;OIB 数据引自 Sun and McDonough (1989)

Fig. 5 Chondrite-normalized REE patterns (a) and primitive mantle-normalized multi-element variation diagrams (b) for the Bachu dykes (normalizing values after McDonough and Sun, 1995)

Reference data sources same as Fig. 3. Also shown is a typical ocean island basalt (OIB) (dashed line) from Sun and McDonough (1989)

CaO 降低,表明有单斜辉石的分离结晶;Al_2O_3 和 MgO 呈负相关,表明斜长石的分离结晶并不明显,与 REE 球粒陨石标准化图解上无明显的 Eu 负异常和微量元素蛛网图上 Sr 轻微的负异常一致。XHZ-10 具有明显的 Eu 负异常,可能经历了明显的斜长石分离结晶。

我们选取 08KT18-9(具有相对高的 MgO = 6.1%, $Fe_2O_3^T$ = 17.2, TiO_2 = 5.2%;Zhang *et al.*, 2010a)为初始成分,在 FMQ(石英-铁橄榄石-磁铁矿)氧逸度和 1kbar 压力条件下,用 MELTS 程序(Ghiorso and Sack, 1995)模拟其分离结晶过程。模拟结果(图 4)显示, Ti-Fe 氧化物(14.3%)、橄榄石(2.3%)和单斜辉石(13.4%)的分离结晶,可以解释巴楚岩墙的成分变化范围。

5.4 同化混染

样品 XHZ-10 中含有大量的新元古代锆石,并且具有低的 Nb/U (10.6) 和 Nb/Zr (0.08) 比值,以及高的 Th/Nb (0.54) 和 La/Nb(2.37)比值,暗示其侵位过程中同化混染了新元古代的基底物质。塔里木新元古代基底具有低的 Nd 同

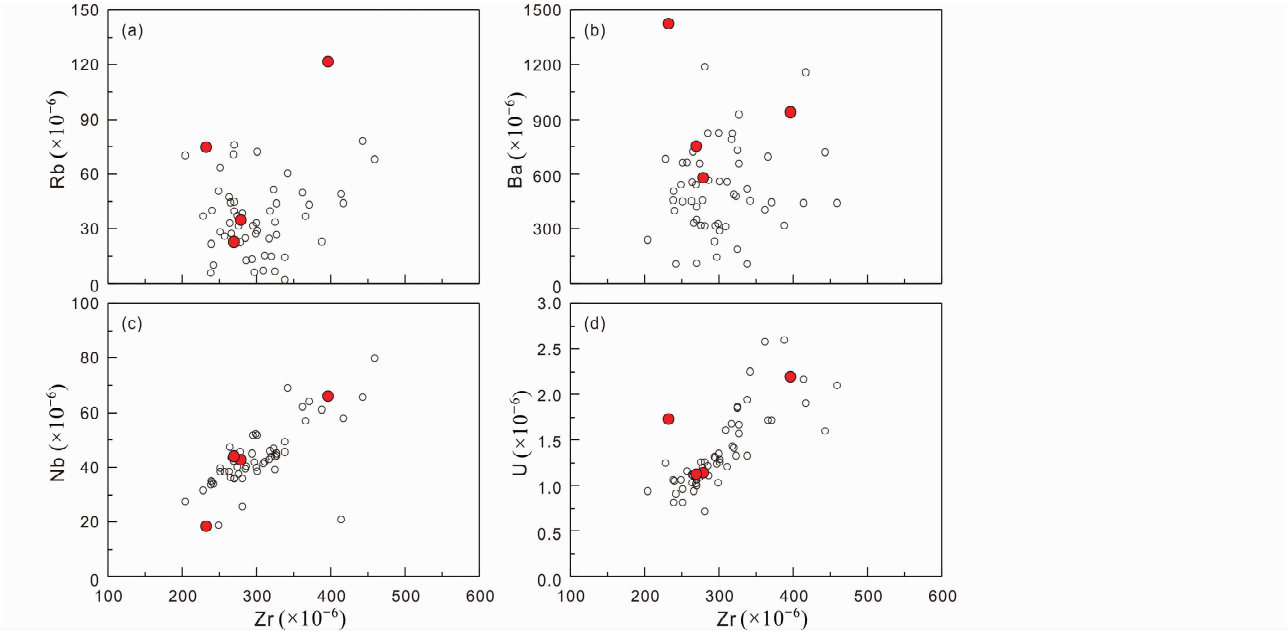


图 6 巴楚岩墙的 Rb-Zr（a）、Ba-Zr（b）、Nb-Zr（c）和 U-Zr（d）图解

图例和文献数据同图 3

Fig. 6 Plots of Rb-Zr (a), Ba-Zr (b), Nb-Zr (c) and U-Zr (d) of the Bachu dykes

Symbols and reference data sources same as Fig. 3

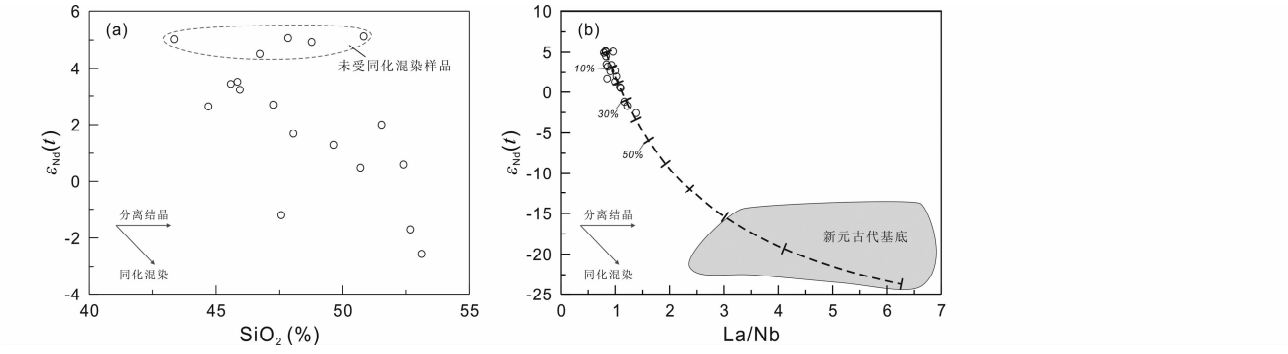


图 7 巴楚岩墙的 $\varepsilon_{Nd}(t)$-SiO_2（a）和 $\varepsilon_{Nd}(t)$-La/Nb（b）图解

图 7a 中虚线范围内的样品具有高的 $\varepsilon_{Nd}(t)$（+4.5 ~ +5.1），为未受到同化混染的样品（详细讨论见 5.4）. 图 7b 中曲线显示简单二单元混合模拟计算结果，端元组成分别为 08KT18-9（Nb = 39.8 × 10^{-6}，La = 33.0 × 10^{-6}，Nd = 42.1 × 10^{-6}，$\varepsilon_{Nd}(280)$ = 5；Zhang *et al.*，2010a）和新元古代基底（Nb = 6.7 × 10^{-6}，La = 42.0 × 10^{-6}，Nd = 26.0 × 10^{-6}，$\varepsilon_{Nd}(280)$ = −23.6；Cao *et al.*，2011；Zhang *et al.*，2007）. 新元古代基底数据引自 Cao *et al.*，2011；Long *et al.*，2011；Zhang *et al.*，2007；Zhu *et al.*，2011. 图例和文献数据同图 3

Fig. 7 Plots of $\varepsilon_{Nd}(t)$-SiO_2 (a) and $\varepsilon_{Nd}(t)$-La/Nb (b) of the Bachu dykes

Results are shown in (b) for assimilation of an uncontaminated sample from the Bahcu dykes (08KT18-9, Zhang *et al.*, 2010a) with Neoproterozoic igneous rocks (Cao *et al.*, 2011; Zhang *et al.*, 2007) as an end-member. Dashed curves with tick marks at 10% indicate the amount of assimilated material relative to 08KT18-9. 08KT18-9 and Neoproterozoic igneous rocks are modeled with 39.8 × 10^{-6} Nb, 33.0 × 10^{-6} La, 42.1 × 10^{-6} Nd, ε_{Nd} (280) of 5, and 6.7 × 10^{-6} Nb, 42.0 × 10^{-6} La, 26.0 × 10^{-6} Nd, $\varepsilon_{Nd}(280)$ of −23.6 respectively. Neoproterozoic basements from: Cao *et al.*, 2011; Long *et al.*, 2011; Zhang *et al.*, 2007; Zhu *et al.*, 2011. Symbols and reference data sources same as Fig. 3

位素比值（−13.3 ~ −23.7，校正至 280Ma）（Cao *et al.*，2011；Hu *et al.*，2000；Xu *et al.*，2005；Zhang *et al.*，2007），幔源岩浆在侵位过程中受到这些物质的同化混染，其 Nd 同位素和微量元素比值会向地壳的方向演化。

大洋玄武岩 Nb/U 平均比值为 52 ± 15（Hofmann，2003；Hofmann *et al.*，1986），明显高于地壳的比值（6.2，Rudnick and Gao，2003），因此低的 Nb/U 比值可以反映地壳的同化混染。巴楚岩墙 Nb/U 比值变化范围较大（9.6 ~ 50.7），暗

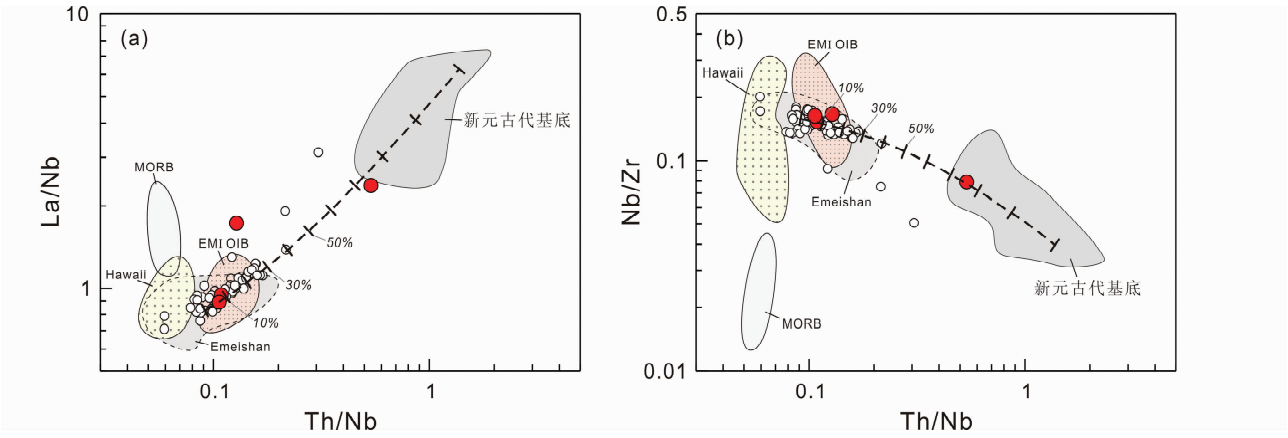


图 8 巴楚岩墙的 La/Nb-Th/Nb(a)和 Nb/Zr-Th/Nb(b)图解

图中曲线显示简单二单元混合模拟计算结果. 端元组成分别为 08KT18-9 ($Th = 3.64 \times 10^{-6}$, $Nb = 39.8 \times 10^{-6}$, $La = 33.0 \times 10^{-6}$, $Zr = 251 \times 10^{-6}$; Zhang *et al.*, 2010a) 和新元古代基底 ($Th = 9.21 \times 10^{-6}$, $Nb = 6.7 \times 10^{-6}$, $La = 42.0 \times 10^{-6}$, $Zr = 169 \times 10^{-6}$; Cao *et al.*, 2011; Zhang *et al.*, 2007). 数据来源: EMI OIB(包括 Wavis Ridge, Gough and Tristan)引自 Salters and Sachi-Kocher (2010), Willbold and Stracke (2006)和 Class and le Roex (2008); Hawaiian OIB 引自 http://georoc.mpch-mainz.gwdg.de/georoc/; MORB 引自 Jenner and O'Neill (2012); 峨嵋山高钛玄武岩引自 Qi and Zhou (2008), Xiao *et al.* (2004), Xu *et al.* (2001)和 Zhang *et al.* (2006). 新元古代基底数据引自: Cao *et al.*, 2011; Long *et al.*, 2011; Zhang *et al.*, 2007; Zhu *et al.*, 2011. 图例和文献数据同图 3

Fig. 8 Plots of La/Nb-Th/Nb (a) and Nb/Zr-Th/Nb of the Bachu dykes

Results are shown for assimilation of an uncontaminated sample from the Bahcu dykes (08KT18-9, Zhang *et al.*, 2010a) with Neoproterozoic igneous rocks (Cao *et al.*, 2011; Zhang *et al.*, 2007) as an end-member. Dashed curves with tick marks at 10% indicate the amount of assimilated material relative to 08KT18-9. 08KT18-9 and Neoproterozoic igneous rocks are modeled with 3.64×10^{-6} Th, 39.8×10^{-6} Nb, 33.0×10^{-6} La, 251×10^{-6} Zr and 9.21×10^{-6} Th, 6.7×10^{-6} Nb, 42.0×10^{-6} La, 169×10^{-6} Zr respectively. Data sources: EMI OIB (including Wavis Ridge, Gough and Tristan) from Salters and Sachi-Kocher (2010), Willbold and Stracke (2006) and Class and le Roex (2008); Hawaiian OIB from http://georoc.mpch-mainz.gwdg.de/georoc/; MORB from Jenner and O'Neill (2012); Emeishan least contaminated high-Ti basalts from Qi *et al.* (2008), Xiao *et al.* (2004), Xu *et al.* (2001) and Zhang *et al.* (2006). Neoproterozoic basements from: Cao *et al.*, 2011; Long *et al.*, 2011; Zhang *et al.*, 2007 and Zhu *et al.*, 2011. Symbols and reference data sources same as Fig. 3

示 Nb/U 比值低的样品可能受到地壳物质的同化混染。巴楚岩墙 $\varepsilon_{Nd}(t)$具有较大的变化范围(−2.6 ~ +5.1)(Zhang *et al.*, 2010a; Zhou *et al.*, 2009)。$\varepsilon_{Nd}(t)$值高的样品(+4.5 ~ +5.1),同时具有低的 Th/Nb(0.06 ~ 0.12)和 La/Nb(0.79 ~ 0.96),和高的 Nb/Zr(0.15 ~ 0.17)比值,暗示 $\varepsilon_{Nd}(t)$值高的样品并未受到地壳同化混染的影响,可以反映源区组成。总体来说,$\varepsilon_{Nd}(t)$随着 SiO_2 和 La/Nb 比值的升高而降低(图 7),和分离结晶与同化混染所预测的趋势一致(Depaolo, 1981),表明 $\varepsilon_{Nd}(t)$值低的样品,是地壳的同化混染所致。简单二单元混合模拟(图 7b 和图 8)结果表明,同化混染 ~30% 的新元古代基底物质可以解释巴楚辉绿岩墙的微量元素和同位素变化范围。需要指出的是,模拟计算中选择的初始样品(08KT18-9, Zhang *et al.*, 2010a)具有比较演化的成分,如果选择更为原始的成分,那么同化混染的量会远小于 30%。

5.5 源区特征

多数巴楚辉绿岩墙与 OIB (Sun and McDonough, 1989)具有非常相似的配分模式(图 5)。而且受同化混染影响较小样品的微量元素比值(如 Th/Nb, La/Nb 和 Nb/Zr),落在 OIB 和峨眉山高钛玄武岩范围内,但是与 MORB 完全不同(图 8)。这些样品的微量元素比值(如 Nb/La = 1.2 ~ 1.4)和 Nd 同位素组成(ε_{Nd} = ~ +5),与形成峨眉山高钛玄武岩推测的地幔柱成分(Nb/La = 1.0 ~ 1.1, ε_{Nd} = +4.6 ~ +4.8; Xu *et al.*, 2001)相似。这些特征暗示巴楚辉绿岩墙可能来自对流地幔源区。

在塔里木盆地西缘的巴楚和皮羌地区,辉绿岩墙在时间和空间上通常与超基性-基性侵入体、正长岩和 A-型花岗岩伴生。根据同位素组成的相似性,这些 A-型花岗岩类被认为和辉绿岩墙以及超基性-基性侵入体具有相似的源区(位荀和徐义刚, 2011; Zhang *et al.*, 2008, 2010a; Zhang and Zou, 2013)。这些 A-型花岗岩类具有非常高的锆石饱和温度(890 ~ 1010℃, Zhang *et al.*, 2010a),是地幔柱相关的侵入体具有的典型特征(钟玉婷和徐义刚, 2009; Shellnutt and Jahn, 2010; Shellnutt and Zhou, 2007; Zhong *et al.*, 2007, 2011)。

5.6 地幔柱-岩石圈相互作用

年龄统计(图 9)表明,塔里木大火成岩省存在明显的两

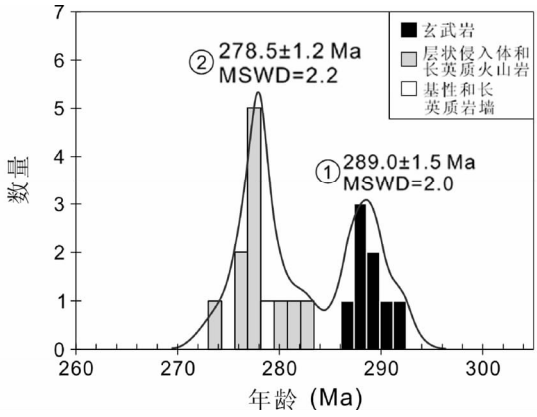


图 9 塔里木大火成岩省岩浆岩年龄分布图

数据来源：杨树峰等，1996，2006；李勇等，2007；张洪安等，2009；余星，2009；上官时迈等，2011；位荀和徐义刚，2011；于峻川等，2011；Tian *et al.*，2010；Yu *et al.*，2011b；Zhang *et al.*，2008，2010a，2012

Fig. 9 Compilation of representative ages of magmatic rocks from the TLIP

Data sources: Li *et al.*, 2007; Shangguan *et al.*, 2011; Tian *et al.*, 2010; Wei and Xu, 2011; Yang *et al.*, 1996, 2006; Yu *et al.*, 2009, 2011a, b; Zhang *et al.*, 2008, 2009, 2010a, 2012

期岩浆活动：玄武岩形成于～290Ma，分布于盆地内部，覆盖面积超过250000km^2；岩墙、超基性-基性侵入岩、长英质侵入岩和火山岩形成较晚（～280Ma），体积小，零散分布于靠近造山带的盆地边缘。并且两期岩浆具有明显不同的地球化学特征和源区组成：～290Ma 玄武岩具有 Nb-Ta 负异常和富集的 Nd 同位素组成（ε_{Nd} = －1.8 ～ －3.9）（姜常义等，2004；Li *et al.*，2012；Yu *et al.*，2011b；Zhang *et al.*，2010a），可能来自于富集的岩石圈地幔源区；辉绿岩墙具有 Nb-Ta 的正异常和亏损的 Nd 同位素组成（ε_{Nd} = ～ +5）（Yang *et al.*，2007；Zhang *et al.*，2010a；Zhou *et al.*，2009），来自于对流地幔。形成如此大规模的玄武岩需要一个巨大的热源提供足够的热使得岩石圈部分熔融。热力学模拟结果表明冷、干的岩石圈地幔不可能发生大规模的熔融形成大陆溢流玄武岩（Arndt and Christensen，1992），但是如果岩石圈地幔先前被挥发分和熔体交代富集，那么在地幔柱的传导加热下在理论上可以发生大程度部分熔融（Gallagher and Hawkesworth，1992；Turner *et al.*，1996）。岩石圈-地幔柱相互作用在塔里木大火成岩省的形成中扮演了很重要的角色：早期的岩浆来自于岩石圈地幔，地幔柱主要提供热源；晚期的岩浆来自于对流地幔，地幔柱提供物源。

任何地球动力学模式，都需要解释塔里木大火成岩省的两期岩浆时间、空间分布特征及它们之间存在的地球化学差异。在塔里木大火成岩省形成过程中，岩石圈-地幔柱的相互作用可能扮演了很重要的角色。现今的塔里木克拉通具有厚、冷的岩石圈地幔（＞140km）（安美建和石耀霖，2006；Liu *et al.*，2004；Priestley *et al.*，2006）。二叠纪以后塔里木

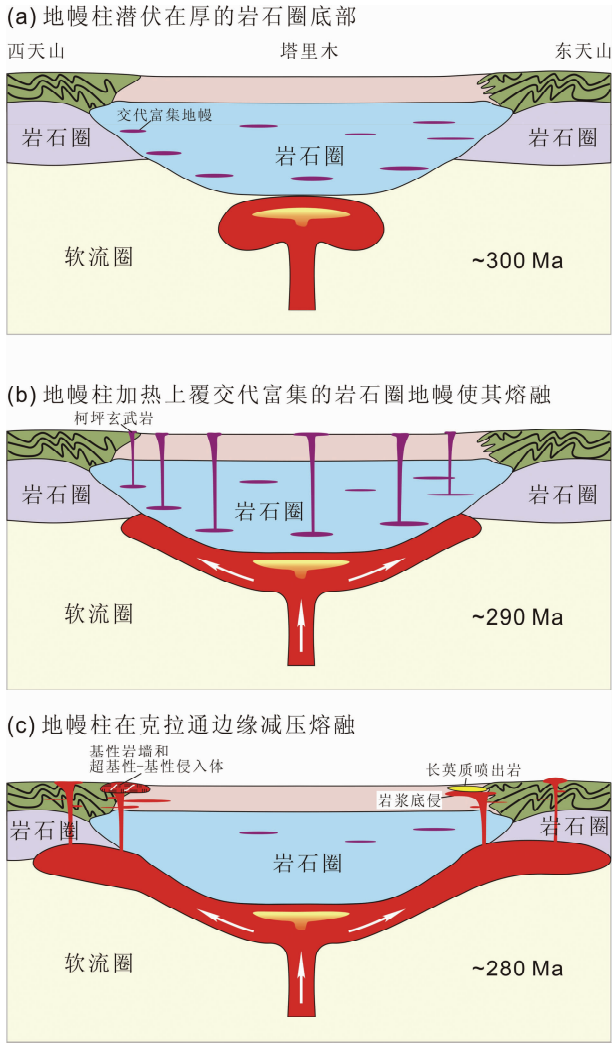


图 10 塔里木大火成岩省形成的动力学示意图（据徐义刚等，2013 修改）

Fig. 10 A cartoon illustrating the formation of the TLIP (modified after Xu *et al.*, 2013)

没有明显的岩浆活动记录（新疆维吾尔自治区地质矿产局，1993），暗示二叠纪后塔里木岩石圈并未发生明显的减薄。如果假设二叠纪时塔里木也具有比较厚的岩石圈地幔（＞140km），当地幔柱上升至岩石圈底部时，巨厚的岩石圈地幔会阻止其继续上升，从而阻碍其减压熔融（Davies，1994；Foley，2008；Jourdan *et al.*，2007；Sleep *et al.*，2002）（图 10a）；但不断积累在岩石圈底部的地幔柱物质会向岩石圈厚度比较薄的边缘地区侧向流动（Sleep *et al.*，2002），并提供足够的热，促使早期交代富集的岩石圈地幔发生部分熔融，形成～290Ma 的溢流玄武岩（图 10b）。

巴楚岩墙具有和 OIB 相似的地球化学特征，暗示它们来自对流软流圈地幔源区。Lebedev *et al.*（2006）认为克拉通下的软流圈地幔物质流动和其导致的克拉通边缘减压熔融，可以解释小体积、分散并且具有 OIB 特征玄武岩的成因。塔

里木盆地~280Ma的岩浆活动以体积小和分布分散为特征,主要分布在盆地的边缘,如塔里木盆地西缘的巴楚和皮羌等地(Zhang *et al.*, 2008, 2010a; Zhang and Zou, 2013)。这些特征和地幔柱物质侧向流动至岩石圈薄的盆地边缘并发生减压熔融模型预测的非常吻合。另外,形成的玄武质岩浆还可以侵位到地壳中,诱发地壳的熔融,形成具有地壳特征的长英质火山岩(图10c)(于峻川等, 2011)。

6 结论

(1)野外地质关系指示巴楚辉绿岩墙属于塔里木大火成岩省的第二期岩浆活动(~280Ma)。巴楚岩墙具有较大的ε_{Nd}值范围(-2.6~+5.1),其中样品XHZ-10含有年龄为717~2480Ma的继承锆石,暗示这些岩墙在侵位过程中同化混染了元古代的基底物质。受混染程度最小的样品具有与OIB十分相似的微量元素特征及亏损的Nd同位素组成(ε_{Nd}=~+5),暗示其来源于富集的软流圈地幔源区,与主要来自富集岩石圈地幔的早期(~290Ma)玄武岩形成鲜明对比。

(2)岩石圈-地幔柱相互作用在塔里木大火成岩省的形成中扮演了很重要的角色:早期(~280Ma)的岩浆来自于岩石圈地幔,地幔柱主要提供热源;晚期的岩浆来自于软流圈地幔,地幔柱提供物源。地幔柱侧向流动模型可以合理地解释塔里木大火成岩省两期岩浆的时间、空间展布特征以及地球化学差异。

References

An MJ and Shi YL. 2006. Review on lithospheric thickness research of the Chinese continent. Earth Science Frontiers, 13(3): 23-30 (in Chinese with English abstract)

Arndt NT and Christensen U. 1992. The role of lithospheric mantle in continental flood volcanism: Thermal and geochemical constraints. Journal of Geophysical Research, 97(B7): 10967-10981

Bryan SE and Ernst RE. 2008. Revised definition of large igneous provinces (LIPs). Earth-Science Reviews, 86(1-4): 175-202

Bureau of Geology and Mineral Resources of Xinjiang Uygur Autonomous Region. 1993. Regional geology of the Xinjiang Uygur Autonomous Region. Beijing: Geological Publishing House: 1-468 (in Chinese)

Campbell IH and Griffiths RW. 1990. Implications of mantle plume structure for the evolution of flood basalts. Earth and Planetary Science Letters, 99(1-2): 79-93

Campbell IH. 2005. Large igneous provinces and the mantle plume hypothesis. Elements, 1(5): 265-269

Cao XF, Lü XB, Liu ST, Zhang P, Gao XA, Chen C and Mo YL. 2011. LA-ICP-MS zircon dating, geochemistry, petrogenesis and tectonic implications of the Dapingliang Neoproterozoic granites at Kuluketage block, NW China. Precambrian Research, 186(1-4): 205-219

Chen HL, Yang SF, Dong CW, Jia CZ, Wei GQ and Wang ZG. 1997. Confirmation of Permian basite zone in Tarim Basin and its tectonic significance. Geochimica, 26(6): 77-87 (in Chinese with English abstract)

Chen MM, Tian W, Zhang ZL, Pan WQ and Song Y. 2010. Geochronology of the Permian basic-intermediate-acidic magma suite from Tarim, Northwest China and its geological implications. Acta Petrologica Sinica, 26(2): 559-572 (in Chinese with English abstract)

Class C and le Roex AP. 2008. Ce anomalies in Gough Island lavas-Trace element characteristics of a recycled sediment component. Earth and Planetary Science Letters, 265(3-4): 475-486

Courtillot V, Davaille A, Besse J and Stock J. 2003. Three distinct types of hotspots in the Earth's mantle. Earth and Planetary Science Letters, 205(3-4): 295-308

Davies GF. 1994. Thermomechanical erosion of the lithosphere by mantle plumes. J. Geophys. Res., 99(B8): 15709-15722

Depaolo DJ. 1981. Trace-element and isotopic effects of combined wallrock assimilation and fractional crystallization. Earth and Planetary Science Letters, 53(2): 189-202

Foley SF. 2008. Rejuvenation and erosion of the cratonic lithosphere. Nature Geoscience, 1(8): 503-510

Gallagher K and Hawkesworth C. 1992. Dehydration melting and the generation of continental flood basalts. Nature, 358(6381): 57-59

Ghiorso MS and Sack RO. 1995. Chemical mass transfer in magmatic processes Ⅳ. A revised and internally consistent thermodynamic model for the interpolation and extrapolation of liquid-solid equilibria in magmatic systems at elevated temperatures and pressures. Contributions to Mineralogy and Petrology, 119(2-3): 197-212

Gibson SA, Thompson RN, Dickin AP and Leonardos OH. 1995. High-Ti and low-Ti mafic potassic magmas: Key to plume-lithosphere interactions and continental flood-basalt genesis. Earth and Planetary Science Letters, 136(3-4): 149-165

Gibson SA, Thompson RN, Leonardos OH, Dickin AP and Mitchell JG. 1999. The limited extent of plume-lithosphere interactions during continental flood-basalt genesis: Geochemical evidence from Cretaceous magmatism in southern Brazil. Contributions to Mineralogy and Petrology, 137(1-2): 147-169

Gibson SA, Thompson RN and Day JA. 2006. Timescales and mechanisms of plume-lithosphere interactions: $^{40}Ar/^{39}Ar$ geochronology and geochemistry of alkaline igneous rocks from the Paraná-Etendeka large igneous province. Earth and Planetary Science Letters, 251(1-2): 1-17

Griffiths RW and Campbell IH. 1990. Stirring and structure in mantle starting plumes. Earth and Planetary Science Letters, 99(1-2): 66-78

Hill RI, Campbell IH, Davies GF and Griffiths RW. 1992. Mantle plumes and continental tectonics. Science, 256(5054): 186-193

Hofmann AW, Jochum KP, Seufert M and White WM. 1986. Nb and Pb in oceanic basalts: New constraints on mantle evolution. Earth and Planetary Science Letters, 79(1-2): 33-45

Hofmann AW. 2003. Sampling mantle heterogeneity through oceanic basalts: Isotopes and trace elements. In: Carlson R (ed.). Treatise on Geochemistry. Pergamon: Elsevier, 2: 61-101

Hu AQ, Jahn BM, Zhang GX, Chen YB and Zhang QF. 2000. Crustal evolution and Phanerozoic crustal growth in northern Xinjiang: Nd isotopic evidence. Part I. Isotopic characterization of basement rocks. Tectonophysics, 328(1-2): 15-51

Jenner FE and O'Neill HSC. 2012. Analysis of 60 elements in 616 ocean floor basaltic glasses. Geochemistry, Geophysics, Geosystems, 13(2): Q02005, doi: 10.1029/2011GC004009

Jiang CY, Zhang PB, Lu DR, Bai KY, Wang YP, Tang SH, Wang JH and Yang C. 2004. Petrology, geochemistry and petrogenesis of the Kalpin basalts and their Nd, Sr and Pb isotopic compositions. Geological Review, 50(5): 492-500 (in Chinese with English abstract)

Jourdan F, Bertrand H, Schärer U, Blichert-Toft J, Féraud G and Kampunzu AB. 2007. Major and trace element and Sr, Nd, Hf, and Pb isotope compositions of the Karoo large igneous province, Botswana-Zimbabwe: Lithosphere vs mantle plume contribution. Journal of Petrology, 48(6): 1043-1077

Lebedev S, Meier T and van der Hilst RD. 2006. Asthenospheric flow and origin of volcanism in the Baikal Rift area. Earth and Planetary Science Letters, 249(3-4): 415-424

Li QL, Li XH, Liu Y, Tang GQ, Yang JH and Zhu WG. 2010. Precise

U-Pb and Pb-Pb dating of Phanerozoic baddeleyite by SIMS with oxygen flooding technique. Journal of Analytical Atomic Spectrometry, 25(7): 1107 – 1113

Li XH, Li ZX, Wingate MTD, Chung SL, Liu Y, Lin GC and Li WX. 2006. Geochemistry of the 755Ma Mundine Well dyke swarm, northwestern Australia: Part of a Neoproterozoic mantle superplume beneath Rodinia? Precambrian Research, 146(1 – 2): 1 – 15

Li XH, Liu Y, Li QL, Guo CH and Chamberlain KR. 2009. Precise determination of Phanerozoic zircon Pb/Pb age by multicollector SIMS without external standardization. Geochemistry, Geophysics, Geosystems, 10(4): Q04010, doi: 10.1029/2009GC002400

Li Y, Su W, Kong P, Qian YX, Zhang KY, Zhang ML, Chen Y, Cai XY and You DH. 2007. Zircon U-Pb ages of the early Permian magmatic rocks in the Tazhong-Bachu region, Tarim basin by LA-ICP-MS. Acta Petrologica Sinica, 23(5): 1097 – 1107 (in Chinese with English abstract)

Li YQ, Li ZL, Sun YL, Santosh M, Langmuir CH, Chen HL, Yang SF, Chen ZX and Yu X. 2012. Platinum-group elements and geochemical characteristics of the Permian continental flood basalts in the Tarim Basin, Northwest China: Implications for the evolution of the Tarim Large Igneous Province. Chemical Geology, 328: 278 – 289

Li ZL, Yang SF, Chen HL, Langmuir CH, Yu X, Lin XB and Li YQ. 2008. Chronology and geochemistry of Taxinan basalts from the Tarim basin: Evidence for Permian plume magmatism. Acta Petrologica Sinica, 24(5): 959 – 970 (in Chinese with English abstract)

Li ZL, Chen HL, Song BA, Li YQ, Yang SF and Yu X. 2011. Temporal evolution of the Permian large igneous province in Tarim Basin in northwestern China. Journal of Asian Earth Sciences, 42(5): 917 – 927

Liu SW, Wang LS, Li C, Li H, Han YB, Jia CZ and Wei GQ. 2004. Thermal-rheological structure of lithosphere beneath the northern flank of Tarim Basin, western China: Implications for geodynamics. Science in China (Series D), Earth Sciences, 47(7): 659 – 672

Long XP, Yuan C, Sun M, Zhao GC, Xiao WJ, Wang YJ, Yang YH and Hu AQ. 2010. Archean crustal evolution of the northern Tarim craton, NW China: Zircon U-Pb and Hf isotopic constraints. Precambrian Research, 180(3 – 4): 272 – 284

Long XP, Yuan C, Sun M, Kröner A, Zhao GC, Wilde S and Hu AQ. 2011. Reworking of the Tarim Craton by underplating of mantle plume-derived magmas: Evidence from Neoproterozoic granitoids in the Kuluketage area, NW China. Precambrian Research, 187(1 – 2): 1 – 14

Ludwig KR. 2003. User's Manual for Isoplot 3.00: A Geochronological Toolkit for Microsoft Excel. Berkeley: Berkeley Geochronology Center Special Publication, 4: 70

McDonough WF and Sun SS. 1995. The composition of the earth. Chemical Geology, 120(3 – 4): 223 – 253

Molzahn M, Reisberg L and Wörner G. 1996. Os, Sr, Nd, Pb, O isotope and trace element data from the Ferrar flood basalts, Antarctica: Evidence for an enriched subcontinental lithospheric source. Earth and Planetary Science Letters, 144(3 – 4): 529 – 545

Pik R, Deniel C, Coulon C, Yirgu G and Marty B. 1999. Isotopic and trace element signatures of Ethiopian flood basalts: Evidence for plume-lithosphere interactions. Geochimica et Cosmochimica Acta, 63(15): 2263 – 2279

Priestley K, Debayle E, McKenzie D and Pilidou S. 2006. Upper mantle structure of eastern Asia from multimode surface waveform tomography. Journal of Geophysical Research-Solid Earth, 111 (B10), doi: 10.1029/2005JB004082

Qi L, Wang CY and Zhou MF. 2008. Controls on the PGE distribution of Permian Emeishan alkaline and peralkaline volcanic rocks in Longzhoushan, Sichuan Province, SW China. Lithos, 106(3 – 4): 222 – 236

Richards MA, Duncan RA and Courtillot VE. 1989. Flood basalts and hot-spot tracks: Plume heads and tails. Science, 246(4926): 103 – 107

Rudnick RL and Gao S. 2003. Composition of the continental crust. In: Rudnick RL (ed.). Treatise on Geochemistry. Pergamon: Elsevier, 3: 1 – 64

Salters VJM and Sachi-Kocher A. 2010. An ancient metasomatic source for the Walvis Ridge basalts. Chemical Geology, 273(3 – 4): 151 – 167

Shangguan SM, Tian W, Li XH, Guan P, Pan M, Chen MM and Pan WQ. 2011. SIMS zircon U-Pb age of a rhyolite layer from the Halahatang area, northern Tarim, NW China: Constraint on the eruption age of major pulse of Tarim flood basalt. Acta Scientiarum Naturalium Universitatis Pekinensis, 47(3): 561 – 564 (in Chinese with English abstract)

Shellnutt JG and Zhou MF. 2007. Permian peralkaline, peraluminous and metaluminous A-type granites in the Panxi district, SW China: Their relationship to the Emeishan mantle plume. Chemical Geology, 243(3 – 4): 286 – 316

Shellnutt JG and Jahn BM. 2010. Formation of the Late Permian Panzhihua plutonic-hypabyssal-volcanic igneous complex: Implications for the genesis of Fe-Ti oxide deposits and A-type granites of SW China. Earth and Planetary Science Letters, 289(3 – 4): 509 – 519

Sláma J, Košler J, Condon DJ, Crowley JL, Gerdes A, Hanchar JM, Horstwood MSA, Morris GA, Nasdala L, Norberg N, Schaltegger U, Schoene B, Tubrett MN and Whitehouse MJ. 2008. Pleš ovice zircon-A new natural reference material for U-Pb and Hf isotopic microanalysis. Chemical Geology, 249(1 – 2): 1 – 35

Sleep NH, Ebinger CJ and Kendall JM. 2002. Deflection of mantle plume material by cratonic keels. In: Fowler CMR, Ebinger CJ and Hawkesworth CJ (eds.). Early Earth: Physical, Chemical and Biological Development. Geological Society, London, Special Publication, 199(1): 135 – 150

Stacey JS and Kramers JD. 1975. Approximation of terrestrial lead isotope evolution by a two-stage model. Earth and Planetary Science Letters, 26(2): 207 – 221

Sun SS and McDonough WF. 1989. Chemical and isotopic systematics of oceanic basalts: Implications for mantle composition and processes. In: Saunders AD and Norry MJ (eds.). Magmatism in Oceanic Basins. Geological Society, London, Special Publications, 42(1): 313 – 345

Tian W, Campbell IH, Allen CM, Guan P, Pan WQ, Chen MM, Yu HJ and Zhu WP. 2010. The Tarim picrite-basalt-rhyolite suite, a Permian flood basalt from Northwest China with contrasting rhyolites produced by fractional crystallization and anatexis. Contributions to Mineralogy and Petrology, 160(3): 407 – 425

Turner S, Hawkesworth C, Gallagher K, Stewart K, Peate D and Mantovani M. 1996. Mantle plumes, flood basalts, and thermal models for melt generation beneath continents: Assessment of a conductive heating model and application to the Paraná. Journal of Geophysical Research, 101(B5): 11503 – 11518

Wei X and Xu YG. 2011. Petrogenesis of Xiaohaizi syenite complex from Bachu area, Tarim. Acta Petrologica Sinica, 27(10): 2984 – 3004 (in Chinese with English abstract)

Wiedenbeck M, Allé P, Corfu F, Griffin WL, Meier M, Oberli F, Von Quadt A, Roddick JC and Speigel W. 1995. Three natural zircon standards for U-Th-Pb, Lu-Hf, trace-element and REE analyses. Geostandards Newsletter, 19(1): 1 – 23

Willbold M and Stracke A. 2006. Trace element composition of mantle end-members: Implications for recycling of oceanic and upper and lower continental crust. Geochemistry, Geophysics, Geosystems, 7 (4): Q04004

Winchester JA and Floyd PA. 1977. Geochemical discrimination of different magma series and their differentiation products using immobile elements. Chemical Geology, 20: 325 – 343

Wolfe CJ, Solomon SC, Laske G, Collins JA, Detrick RS, Orcutt JA, Bercovici D and Hauri EH. 2009. Mantle shear-wave velocity structure beneath the Hawaiian hot spot. Science, 326 (5958): 1388 – 1390

Xiao L, Xu YG, Mei HJ, Zheng YF, He B and Pirajno F. 2004. Distinct mantle sources of low-Ti and high-Ti basalts from the western Emeishan large igneous province, SW China: Implications for plume-lithosphere interaction. Earth and Planetary Science Letters, 228(3-4): 525-546

Xu B, Jian P, Zheng HF, Zou HB, Zhang LF and Liu DY. 2005. U-Pb zircon geochronology and geochemistry of Neoproterozoic volcanic rocks in the Tarim Block of Northwest China: Implications for the breakup of Rodinia supercontinent and Neoproterozoic glaciations. Precambrian Research, 136(2): 107-123

Xu YG, Chung SL, Jahn BM and Wu GY. 2001. Petrologic and geochemical constraints on the petrogenesis of Permian-Triassic Emeishan flood basalts in southwestern China. Lithos, 58(3-4): 145-168

Xu YG. 2002. Evidence for crustal components in the mantle and constraints on crustal recycling mechanisms: Pyroxenite xenoliths from Hannuoba, North China. Chemical Geology, 182(2-4): 301-322

Xu YG, He B, Chung SL, Menzies MA and Frey FA. 2004. Geologic, geochemical, and geophysical consequences of plume involvement in the Emeishan flood-basalt province. Geology, 32(10): 917-920

Xu YG, He B, Luo ZY and Liu HQ. 2013. Study on mantle plume and large igneous provinces in China: An overview and perspectives. Bulletin of Mineralogy, Petrology and Geochemistry, 32(1): 25-39 (in Chinese with English abstract)

Yang SF, Chen HL, Dong CW, Jia CZ and Wang ZG. 1996. The discovery of Permian syenite inside Tarim basin and its geodynamic significance. Geochimica, 25(2): 121-128 (in Chinese with English abstract)

Yang SF, Li ZL, Chen HL, Xiao WJ, Yu X, Lin XB and Shi XG. 2006. Discovery of a Permian quartz syenitic porphyritic dyke from the Tarim basin and its tectonic implications. Acta Petrologica Sinica, 22(5): 1405-1412 (in Chinese with English abstract)

Yang SF, Li ZL, Chen HL, Santosh M, Dong CW and Yu X. 2007. Permian bimodal dyke of Tarim Basin, NW China: Geochemical characteristics and tectonic implications. Gondwana Research, 12(1-2): 113-120

Yu JC, Mo XX, Dong GC, Yu XH, Xing FC, Li Y and Huang XK. 2011a. Felsic volcanic rocks from northern Tarim, NW China: Zircon U-Pb dating and geochemical characteristics. Acta Petrologica Sinica, 27(7): 2184-2194 (in Chinese with English abstract)

Yu X. 2009. Magma evolution and deep geological processes of early Permian Tarim large igneous province. Ph. D. Dissertation. Hangzhou: Zhejiang University (in Chinese with English summary)

Yu X, Yang SF, Chen HL, Chen ZQ, Li ZL, Batt GE and Li YQ. 2011b. Permian flood basalts from the Tarim Basin, Northwest China: SHRIMP zircon U-Pb dating and geochemical characteristics. Gondwana Research, 20(2-3): 485-497

Zhang CL, Li XH, Li ZX, Lu SN, Ye HM and Li HM. 2007. Neoproterozoic ultramafic-mafic-carbonatite complex and granitoids in Quruqtagh of northeastern Tarim Block, western China: Geochronology, geochemistry and tectonic implications. Precambrian Research, 152(3-4): 149-169

Zhang CL, Li XH, Li ZX, Ye HM and Li CN. 2008. A permian layered intrusive complex in the western tarim block, northwestern China: Product of a ca. 275Ma mantle plume? Journal of Geology, 116(3): 269-287

Zhang CL, Xu YG, Li ZX, Wang HY and Ye HM. 2010a. Diverse Permian magmatism in the Tarim Block, NW China: Genetically linked to the Permian Tarim mantle plume? Lithos, 119(3-4): 537-552

Zhang CL and Zou HB. 2013. Permian A-type granites in Tarim and western part of Central Asian Orogenic Belt (CAOB): Genetically related to a common Permian mantle plume? Lithos, 172-173: 47-60

Zhang DY, Zhou TF, Yuan F, Jowitt SM, Fan Y and Liu S. 2012. Source, evolution and emplacement of Permian Tarim Basalts: Evidence from U-Pb dating, Sr-Nd-Pb-Hf isotope systematics and whole rock geochemistry of basalts from the Keping area, Xinjiang Uygur Autonomous Region, Northwest China. Journal of Asian Earth Sciences, 49: 175-190

Zhang HA, Li YJ, Wu GY, Su W, Qian YX, Meng QL, Cai XY, Han LJ, Zhao Y and Liu YL. 2009. Isotopic geochronology of Permian igneous rocks in the Tarim Basin. Chinese Journal of Geology, 44(1): 137-158 (in Chinese with English abstract)

Zhang SB. 2003. A Guide to the Stratigraphic Investigation on the Periphery of the Tarim Basin. Beijing: Petroleum Industry Press: 1-280 (in Chinese)

Zhang YT, Liu JQ and Guo ZF. 2010b. Permian basaltic rocks in the Tarim basin, NW China: Implications for plume-lithosphere interaction. Gondwana Research, 18(4): 596-610

Zhang ZC, Mahoney JJ, Mao JW and Wang FS. 2006. Geochemistry of picritic and associated basalt flows of the western Emeishan flood basalt province, China. Journal of Petrology, 47(10): 1997-2019

Zhang ZL, Qin QM, Tian W, Cao B, Li BS and Chen MM. 2008. Emplacement characteristics and spatial distribution of Permian Mazhartager basic dike swarms in Bachu area, Tarim basin. Acta Petrologica Sinica, 24(10): 2273-2280 (in Chinese with English abstract)

Zhong H, Zhu WG, Chu ZY, He DF and Song XY. 2007. Shrimp U-Pb zircon geochronology, geochemistry, and Nd-Sr isotopic study of contrasting granites in the Emeishan large igneous province, SW China. Chemical Geology, 236(1-2): 112-133

Zhong H, Campbell IH, Zhu WG, Allen CM, Hu RZ, Xie LW and He DF. 2011. Timing and source constraints on the relationship between mafic and felsic intrusions in the Emeishan large igneous province. Geochimica et Cosmochimica Acta, 75(5): 1374-1395

Zhong YT and Xu YG. 2009. Characteristics of plume-related A-type granites: An example from the Emeishan large igneous province. Journal of Jilin University (Earth Science Edition), 39(5): 828-838 (in Chinese with English abstract)

Zhou MF, Zhao JH, Jiang CY, Gao JF, Wang W and Yang SH. 2009. OIB-like, heterogeneous mantle sources of Permian basaltic magmatism in the western Tarim Basin, NW China: Implications for a possible Permian large igneous province. Lithos, 113(3-4): 583-594

Zhu WB, Zheng BH, Shu LS, Ma DS, Wu HL, Li YX, Huang WT and Yu JJ. 2011. Neoproterozoic tectonic evolution of the Precambrian Aksu blueschist terrane, northwestern Tarim, China: Insights from LA-ICP-MS zircon U-Pb ages and geochemical data. Precambrian Research, 185(3-4): 215-230

附中文参考文献

安美建, 石耀霖. 2006. 中国大陆岩石圈厚度分布研究. 地学前缘, 13(3): 23-30

陈汉林, 杨树峰, 董传万, 贾承造, 魏国齐, 汪振国. 1997. 塔里木盆地二叠纪基性岩带的确定及大地构造意义. 地球化学, 26(6): 77-87

陈咪咪, 田伟, 张自力, 潘文庆, 宋宇. 2010. 塔里木二叠纪基性-中性-酸性岩浆岩的年代学及其地质意义. 岩石学报, 26(2): 559-572

姜常义, 张蓬勃, 卢登蓉, 白开寅, 王瑶培, 唐索寒, 王进辉, 杨淳. 2004. 柯坪玄武岩的岩石学、地球化学、Nd、Sr、Pb 同位素组成与岩石成因. 地质论评, 50(5): 492-500

李勇, 苏文, 孔屏, 钱一雄, 张克银, 张明利, 陈跃, 蔡习尧, 尤东华. 2007. 塔里木盆地塔中-巴楚地区早二叠世岩浆岩的 LA-ICP-MS 锆石 U-Pb 年龄. 岩石学报, 23(5): 1097-1107

厉子龙, 杨树峰, 陈汉林, Langmuir CH, 余星, 林秀彬, 励音骐, 2008. 塔西南玄武岩年代学和地球化学特征及其对二叠纪地幔

柱岩浆演化的制约. 岩石学报, 24(5): 959 – 970

上官时迈,田伟,李献华,关平,潘懋,陈咪咪,潘文庆. 2011. 塔北哈拉哈塘流纹岩的离子探针锆石 U-Pb 年代学:对塔里木溢流玄武岩主期喷发时代的约束. 北京大学学报(自然科学版),47(3): 561 – 564

位荀, 徐义刚. 2011. 塔里木巴楚小海子正长岩杂岩体的岩石成因探讨. 岩石学报, 27(10): 2984 – 3004

新疆维吾尔自治区地质矿产局. 1993. 新疆维吾尔自治区区域地质志. 北京: 地质出版社, 1 – 468

徐义刚, 何斌, 罗震宇, 刘海泉. 2013. 我国大火成岩省和地幔柱研究进展与展望. 矿物岩石地球化学通报, 32(1): 25 – 39

杨树峰, 陈汉林, 董传万, 贾承造, 汪振国. 1996. 塔里木盆地二叠纪正长岩的发现及其地球动力学意义. 地球化学, 25(2): 121 – 128

杨树峰, 厉子龙, 陈汉林, 肖文交, 余星, 林秀斌, 施锡桂. 2006. 塔里木二叠纪石英正长斑岩岩墙的发现及其构造意义. 岩石学报, 22(5): 1405 – 1412

于峻川, 莫宣学, 董国臣, 喻学惠, 邢凤存, 李勇, 黄行凯. 2011. 塔里木北部二叠纪长英质火山岩年代学及地球化学特征. 岩石学报, 27(7): 2184 – 2194

余星. 2009. 塔里木早二叠世大火成岩省的岩浆演化与深部地质作用. 博士学位论文. 杭州: 浙江大学

张洪安, 李曰俊, 吴根耀, 苏文, 钱一雄, 孟庆龙, 蔡习尧, 韩利军, 赵岩, 刘亚雷. 2009. 塔里木盆地二叠纪火成岩的同位素年代学. 地质科学, 44(1): 137 – 158

张师本. 2003. 塔里木盆地周缘地层考察指南. 北京: 石油工业出版社, 1 – 280

张自力, 秦其明, 田伟, 曹宝, 李百寿, 陈咪咪. 2008. 塔里木麻扎尔塔格基性岩墙群的侵位特征和空间分布规律研究. 岩石学报, 24(10): 2273 – 2280

钟玉婷,徐义刚. 2009. 与地幔柱有关的 A 型花岗岩的特点:以峨眉山大火成岩省为例. 吉林大学学报(地球科学版), 39(5): 828 – 838